1998

The Effect of Particle Size on the Discharge Performance of a Nickel-Metal Hydride Cell

Jussi M. Heikonen

Harry J. Ploehn
University of South Carolina - Columbia, ploehn@cec.sc.edu

Ralph E. White
University of South Carolina - Columbia, white@cec.sc.edu

Publication Info

Journal of the Electrochemical Society, 1998, pages 1840-1848.

57. T. R. Beck, *Electrochem. Acta*, **18**, 815 (1973).
58. T. R. Beck, *J. Electrochem. Soc.*, **115**, 890 (1968).
59. H. J. Rätzer-Scheibe, in *Passivity of Metals and Semiconductors*, M. Froment, Editor, p. 731, Elsevier Science Publishers, Amsterdam (1983).
60. H. J. Rätzer-Scheibe, in *Proceedings of the 8th International Congress on Corrosion*, p. 212, Mainz, Germany (1981).
61. H. J. Rätzer-Scheibe and H. Buhl, in *Titanium Science and Technology, Proceedings of the 5th International Conference on Titanium*, Vol. 4, G. Lütjering, U. Zwicker, and W. Bunk, Editors, p. 2641, Deutsche Gesselschaft für Mettalkunde, Germany (1984).
62. T. R. Beck, *Corrosion*, **30**, 408 (1974).
63. M. A. Gaudett, Ph.D. Dissertation, University of Virginia, Charlottesville, VA (1997).
64. M. Prazák and M. Holinka, in *Stress Corrosion Cracking and Hydrogen Embrittlement of Iron Base Alloys*, R. W. Staehle, J. Hochmann, R. D. McCright, and J. E. Slater, Editors, p. 1020, NACE, Houston, TX (1977).
65. R. E. Adams and E. von Tiesenhausen, in *Fundamentals of Stress Corrosion Cracking*, R. W. Staehle, A. J. Forty, and D. VanRooyen, Editors, p. 691, NACE, Houston, TX (1969).
66. R. J. H. Wanhill, *Br. Corros. J.*, **10**, 69 (1975).
67. D. T. Powell and J. C. Scully, in *Fracture 1969*, P. L. Pratt, Editor, p. 406, Chapman and Hall, London (1969).
68. R. Stickler and S. Barnartt, *J. Electrochem. Soc.*, **109**, 343 (1962).
69. D. Tromans and J. Nutting, in *Fracture*, J. Gilman, Editor, p. 637, Interscience, NY (1963).
70. F. P. Ford, *Met. Sci.*, 326 (1978).
71. H. J. Pearson, G. T. Burstein, and R. C. Newman, *J. Electrochem. Soc.*, **128**, 2297 (1981).
72. D. G. Kolman and J. R. Scully, in *Effects of the Environment on the Initiation of Crack Growth*, ASTM STP 1298, W. A. Van der Sluys, R. S. Piascik, and R. Zawierucha, Editors, p. 61, ASTM, Philadelphia, PA (1997).
73. J. Newman, *Electrochemical Systems*, p. 4, Prentice-Hall, Englewood Cliffs, NJ (1973).
74. R. C. Newman, *Corrosion*, **50**, 682 (1994).

The Effect of Particle Size on the Discharge Performance of a Nickel-Metal Hydride Cell

Jussi M. Heikonen*

Center for Scientific Computing, Tietotie 6, FIN-02101 Espoo, Finland

Harry J. Ploehn and Ralph E. White**

Department of Chemical Engineering, University of South Carolina, Columbia, South Carolina 29208, USA

ABSTRACT

We investigate the effect of particle size on the discharge performance of a nickel–metal hydride cell with a mathematical model. Electrodes with uniform as well as with nonuniform particle sizes are studied. With uniform particle size, the dependence of the particle-to-particle resistance on the particle size is taken into account. The optimal particle size depends on the discharge rate. Moreover, we show that under certain conditions it is advantageous to use a nonuniform particle size. In general, the higher the discharge current density, the more the particle size affects the electrode performance.

Introduction

In this article we study the effect of particle size on the discharge performance of a nickel–metal hydride cell. We use a mathematical model to describe the behavior of the metal hydride (MH) electrode in constant-current discharge and perform numerical simulations for various particle sizes.

Normally, when a MH electrode is cycled, the particle size decreases due to fracturing caused by absorption and desorption of hydrogen. Thus, it is somewhat difficult to control the particle size in an electrode. However, it has been shown that microencapsulation of the particles with palladium, for example, reduces this disintegration and also increases the corrosion resistance of the alloy (see Ref. 1). Hence the particle size and active surface area of such an electrode can be assumed constant at least for a certain period of the electrode lifetime.

Here we consider an electrode consisting of microencapsulated MH particles, because without the above-mentioned stabilizing effects it would not be meaningful to simulate an electrode with a certain specified particle size.

In earlier work, see Ref. 2–4 for example, only electrodes having constant particle size throughout have been studied. We systematically investigate the effects of varying the particle size in such an electrode using a model in which the bulk conductivity of the solid phase depends on the particle size. Additionally, we are interested in electrodes where the particle size is allowed to vary from place to place. In order to be able to compare the results in a reasonable way, we study electrodes having the same capacity, porosity, and thickness.

In the following sections we first present the mathematical model and define some auxiliary quantities. Then simulations with various constant particle sizes are performed and the results are discussed and analyzed. Finally, we show how the electrode performance can be improved under certain conditions by using nonuniform particle size.

Mathematical Model

In this section we briefly introduce the cell geometry and the model equations. We consider a cell in which a thick porous MH electrode is placed next to a thin counter electrode, which in this case is a nickel electrode. The electrolyte is an aqueous solution of KOH.

We neglect water production during discharge and assume that the concentration of water is independent of both time and position. In a real electrode, however, water production has an effect on polarization, especially at high current pulses.

The length of the MH electrode is L. The nickel electrode is located at $x = 0$, and a current collector is placed at $x = L$. The cell geometry is schematically shown in Fig. 1a. Both the nickel electrode and the separator between the electrodes are assumed to be infinitely thin.

Let ϵ be the porosity or the void volume fraction of the electrode and denote the specific surface density of MH particles by α (m^2/m^3). In all our simulations the porosity

* Electrochemical Society Student Member.
** Electrochemical Society Active Member.

is constant, but in some cases the particle radius and the surface area density are allowed to change within the electrode. Since we assume that the MH particles are spherical, porosity and surface area density are related by

$$\alpha(x) = \frac{3(1-\epsilon)}{R_{MH}(x)} \quad [1]$$

where R_{MH} is the local radius of MH particles.

Let c (mol/m^3) and h (mol/m^3) be the concentrations of hydroxyl ions in the electrolyte and hydrogen in the MH particles, respectively. The electric potentials in the electrolyte and in the solid phase are denoted by ϕ (V) and φ (V). Moreover, the local microreaction-rate density, that is, the reaction rate density on MH particle surfaces, is denoted by j (mol/m^{2}s).

In the following sections we use the abbreviations

$$\sigma = \epsilon^{1.5}\sigma^{free},\ \sigma_{\pm} = \epsilon^{1.5}\sigma_{\pm}^{free},\ D = \epsilon^{1.5}D^{free},\ D_{\pm} = \epsilon^{1.5}D_{\pm}^{free} \quad [2]$$

for the effective conductivities and the diffusion coefficients in the porous electrode, see Ref. 5. In these equations, the factor $\epsilon^{1.5}$ includes both the effects of porosity (ϵ) and tortuosity ($\epsilon^{0.5}$).

Mass transport in the electrolyte.—We use dilute solution theory from Ref. 6 with concentration-dependent diffusion coefficients and conductivities. This yields

$$\epsilon\frac{\partial}{\partial t}c = -\frac{\partial}{\partial x}\left(-D(c)\frac{\partial}{\partial x}c\right) - t_+\alpha(x)j \quad [3]$$

$$0 = -\frac{\partial}{\partial x}\left\{-[D_-(c) - D_+(c)]\frac{\partial}{\partial x}c + \frac{\sigma(c)}{F}\frac{\partial}{\partial x}\phi\right\} - \alpha(x)j \quad [4]$$

where D is the effective integral diffusion coefficient of the electrolyte and D_+ and D_- are the effective ionic diffusion coefficients of K^+ and OH^- ions, respectively. Furthermore, σ is the effective conductivity of the electrolyte and t_+ is the transference number of the positive ions.

Denote the discharge flux density by J (mol/m^2 s). The boundary conditions

$$\left[-D(c)\frac{\partial}{\partial x}c\right](t,0) = t_+J \quad [5]$$

$$\left[-D(c)\frac{\partial}{\partial x}c\right](t,L) = 0 \quad [6]$$

$$\left\{-[D_-(c) - D_+(c)]\frac{\partial}{\partial x}c + \frac{\sigma(c)}{F}\frac{\partial}{\partial x}\phi\right\}(t,0) = J \quad [7]$$

$$\left\{-[D_-(c) - D_+(c)]\frac{\partial}{\partial x}c + \frac{\sigma(c)}{F}\frac{\partial}{\partial x}\phi\right\}(t,L) = 0 \quad [8]$$

model the nickel electrode at $x = 0$ as a source of hydroxyl ions and a closed end at $x = L$.

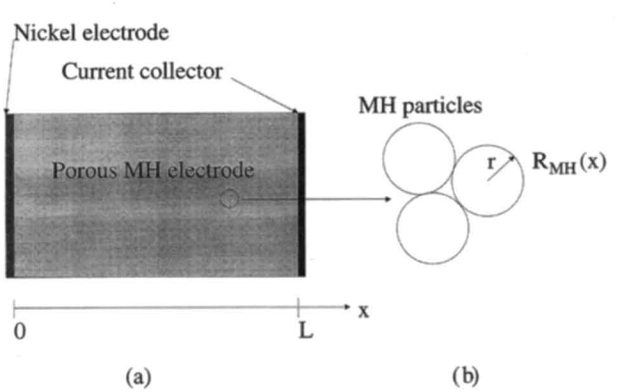

Fig. 1. (a) Scheme of the model geometry. The counter electrode is located at $x = 0$ and the current collector is placed at $x = L$. (b) MH particles are assumed to be spherical with a radius depending on the position in the electrode.

The initial condition for the electrolyte concentration is

$$c(0, x) = c_0 \quad [9]$$

Hydrogen diffusion in MH particles.—We assume that the MH particles are spherical (Fig. 1b). As mentioned earlier, particle radius R_{MH} is a function of x, the position in the electrode.

In a simplified description, the hydrogen concentration satisfies the diffusion equation

$$\frac{\partial}{\partial t}h = D_H\frac{1}{r^2}\frac{\partial}{\partial r}\left(r^2\frac{\partial}{\partial r}h\right) \quad [10]$$

for $0 < r < R_{MH}(x)$ and the boundary conditions

$$-D_H\frac{\partial}{\partial r}h(t,x,0) = 0 \quad [11]$$

$$-D_H\frac{\partial}{\partial r}h[t,x,R_{MH}(x)] = j \quad [12]$$

where D_H is the diffusion coefficient of hydrogen.

The initial condition is constant concentration across the electrode

$$h(0,x,r) = h_0 \quad [13]$$

When defining the reaction rate density on the MH particles, we need h_s, the concentration of the hydrogen on a particle surface. This is simply

$$h_s(t,x) = h[t,x,R_{MH}(x)] \quad [14]$$

Electric current in the solid phase.—Using Ohm's law we get an equation for the potential φ

$$-\frac{\partial}{\partial x}\left[\kappa(x)\frac{\partial}{\partial x}\varphi\right] = -F\alpha(x)j \quad [15]$$

Here κ is the effective conductivity of the solid phase.

We now develop a simple model to describe how the conductivity of the solid phase depends on the particle size. Both the MH alloy of the particles and the contact resistances between the particles contribute to the overall resistance of the matrix. In this section we assume that the MH particles are arranged in a simple cubic lattice oriented with the x axis. Thus the successive layers of MH particles are connected in series with contact resistances between the particles.

There are

$$(1-\epsilon)\left(\frac{4}{3}\pi R_{MH}^3\right)^{-1} \quad [16]$$

MH particles per unit volume. Since the particles form a cubic lattice this means that there are

$$(1-\epsilon)^{1/3}\left(\frac{4}{3}\pi R_{MH}^3\right)^{-1/3} = \left(\frac{3(1-\epsilon)}{4\pi}\right)^{1/3}\frac{1}{R_{MH}} \quad [17]$$

layers of particles per unit distance. Clearly, the contact resistivity should be proportional to this. The contact resistivity should also be inversely proportional to the contact area per total cross-sectional area. If we assume that the contact area of a particle is a fixed fraction of its surface area, then the contact area density is independent of R_{MH}. As a result we may write for the effective conductivity

$$\kappa(x) = (1-\epsilon)\left(\frac{1}{\kappa_0} + \frac{[3(1-\epsilon)/4\pi]^{1/3}\rho_c}{R_{MH}(x)}\right)^{-1} \quad [18]$$

$$\approx \frac{R_{MH}(x)(1-\epsilon)^{2/3}}{(3/4\pi)^{1/3}\rho_c} \quad [19]$$

where κ_0 is the conductivity of the MH alloy and ρ_c (Ω m^2) is the contact resistivity coefficient. The factor $(1-\epsilon)$ before the expression in the parentheses in Eq. 18 is included to compensate for the porosity so that an effective value is obtained.

As metals are generally good conductors, it is reasonable to assume that the resistance of the solid phase is mainly due to the interparticle contacts. Moreover, the value of the conductivity of the MH alloy, κ_0, is not known. Thus we assume that $1/\kappa_0$ is considerably smaller than the contact resistance term in Eq. 18. Ignoring $1/\kappa_0$ yields the approximative equation, Eq. 19. These expressions can also be viewed as phenomenological models which have the property that the conductivity decreases as the particle size decreases. For fixed porosity, the amount of MH alloy in the electrode is constant. Decreasing the particle size results in more particles and interparticle contacts, which decrease the electric conductivity.

Finally, the boundary conditions for electric current in the solid are

$$\kappa(0)\frac{\partial}{\partial x}\varphi(t,0) = 0 \qquad [20]$$

$$\kappa(L)\frac{\partial}{\partial x}\varphi(t,L) = FJ \qquad [21]$$

which model an insulated end at $x = 0$ and the current collector at $x = L$, respectively. We arbitrarily choose

$$\varphi(t, 0) = 0 \qquad [22]$$

to fix the potentials.

Reaction kinetics.—We use a simple Butler–Volmer equation to model the kinetics of the reaction

$$MH_{ads} + OH^- \rightleftharpoons e^- + H_2O + M \qquad [23]$$

The microreaction-rate density j (mol/m^{2}s) is given by

$$j = k_a c h_s \exp\left(\frac{0.5F}{RT}V\right) - k_c(\beta h_0 - h_s)\exp\left(-\frac{0.5F}{RT}V\right) \qquad [24]$$

where $V = \varphi - \phi$, the potential difference between the electrolyte and the solid phase, is measured with a Hg/HgO reference electrode and h_s is the surface concentration of hydrogen as defined earlier in the section on Hydrogen diffusion in MH particles.

The parameter $\beta > 1$ describes the relative maximal charging level of the electrode. If we had $\beta = 1$ in Eq. 24, the equilibrium potential of the electrode at $t = 0$ would be minus infinity. Choosing $\beta > 1$ means that initially the electrode is not charged quite to its full capacity.

The reaction rates k_a and k_c are related to the exchange current density i_0 (A/m^2) and the equilibrium potential $V_0(c_0, h_0)$ of the electrode at its initial state by

$$k_a = \frac{i_0}{Fc_0h_0}\exp\left(-\frac{0.5F}{RT}V_0(c_0,h_0)\right) \qquad [25]$$

$$k_c = \frac{i_0}{F(\beta-1)h_0}\exp\left(\frac{0.5F}{RT}V_0(c_0,h_0)\right) \qquad [26]$$

Numerical solution of the model equations.—The model equations are solved numerically with PDE2D[7] using a method that allows handling pseudo-two-dimensional problems.[8] As PDE2D solves time-dependent PDE problems, no preliminary spatial discretization is needed.

Potential Losses and Ragone Plots

We define Φ_{MH}, the electrode potential of the MH electrode, to be the potential difference between the current collector and the electrolyte between the electrodes measured with a Hg/HgO reference electrode. That is

$$\Phi_{MH}(t) = \varphi(t, L) - \phi(t, 0) \qquad [27]$$

Assuming that Φ_{Ni}, the electrode potential of the nickel electrode, is constant the cell potential E is then given by

$$E(t) = \Phi_{Ni} - \Phi_{MH}(t) \qquad [28]$$

Next we define the equilibrium potentials for the MH electrode. These are obtained from the Butler–Volmer equation, Eq. 24, by setting $j = 0$ and using appropriate electrolyte and hydrogen concentrations. Let

$$V_0(c_0, h_0) = \frac{RT}{F}\ln\left\{\frac{k_c}{k_a}\frac{\beta h_0 - h_s}{ch_s}\right\} \qquad [29]$$

Thus the local momentary equilibrium potential is

$$V_0[c(t,x), h_s(t,x)] = \frac{RT}{F}\ln\left\{\frac{k_c}{k_a}\frac{\beta h_0 - h_s(t,x)}{c(t,x)h_s(t,x)}\right\} \qquad [30]$$

and the steady-state open-circuit equilibrium potential is

$$V_0[c_0, (1 - t/t_{max})h_0] = \frac{RT}{F}\ln\left\{\frac{k_c}{k_a}\frac{[\beta - (1 - t/t_{max})]h_0}{c_0(1 - t/t_{max})h_0}\right\} \qquad [31]$$

where

$$t_{max} = \frac{(1-\epsilon)Lh_0}{J} \qquad [32]$$

is the maximal theoretical discharge time for constant-current discharge. For later use we define the state of discharge at the given time t as

$$SOD(t) = t/t_{max} \qquad [33]$$

Note that

$$V_0(c_0, h_0) = \frac{RT}{F}\ln\left\{\frac{k_c}{k_a}\frac{\beta - 1}{c_0}\right\} \qquad [34]$$

which again shows that we must choose $\beta > 1$, as mentioned in the section on Reaction kinetics.

We are now ready to define V_{loss}, the total potential loss in the MH electrode. We set

$$V_{loss}(t) = \Phi_{MH}(t) - V_0[c_0, (1 - t/t_{max})h_0] \qquad [35]$$

To analyze the electrode performance we use the averaged potential losses presented in Ref. 4. More precisely, the total potential loss in the electrode is first expressed as the sum of the local potential loss in the electrolyte η_l, the local potential loss in the solid η_s, the local reaction overpotential η_r, and the local concentration polarization loss η_p. These are defined as follows

$$\eta_l(t, x) = \phi(t, x) - \phi(t, 0) \qquad [36]$$

$$\eta_s(t, x) = \varphi(t, L) - \varphi(t, x) \qquad [37]$$

$$\eta_r(t, x) = V(t, x) - V_0[c(t, x), h_s(t, x)] \qquad [38]$$

$$\eta_p(t, x) = V_0[c(t, x), h_s(t, x)] - V_0[c_0, (1 - t/t_{max})\, h_0] \qquad [39]$$

Both the electrolyte and hydrogen concentration polarization contribute to η_p.

We then define the averaged losses. For example, the averaged potential loss in the electrolyte, $\bar{\eta}_l$, is given by

$$\bar{\eta}_l(t) = \frac{\int_0^L \alpha(\xi)j(t,\xi)\eta_l(t,\xi)d\xi}{J} \qquad [40]$$

and the remaining three averaged losses are defined similarly. It is easy to see that the equation

$$V_{loss}(t) = \bar{\eta}_l(t) + \bar{\eta}_s(t) + \bar{\eta}_r(t) + \bar{\eta}_p(t) \qquad [41]$$

holds for all $t > 0$, which means that the averaged losses sum up correctly.

In Ref. 9 the averaged reaction rate density was introduced. This is a useful quantity that is related to the uniformity of the reaction as a function of time. If the reaction is completely spread out we have

$$\alpha(x)j(t, x) = \frac{J}{L} \qquad [42]$$

To measure the uniformity of the reaction we consider the integral

$$\int_0^L \left(\frac{J}{L} - \alpha(\xi) j(t,\xi) \right)^2 d\xi = \int_0^L [\alpha(\xi) j(t,\xi)]^2 d\xi - \frac{J^2}{L} \quad [43]$$

where we used the conservation of charge equation

$$\int_0^L \alpha(\xi) j(t,\xi) d\xi = J \quad [44]$$

which follows from the model equations. Thus, the lower the value of

$$M(t) = \frac{L \int_0^L [\alpha(\xi) j(t,\xi)]^2 d\xi}{J^2} \quad [45]$$

the more evenly spread out the reaction in the MH electrode is. Clearly, $M \geq 1$. We call M the measure of the uniformity of the reaction.

To evaluate different electrodes we use Ragone plots in which the energy density E_S (J/m^3) is plotted vs. the average power density P_S (W/m^3). These are defined as follows

$$E_S = \frac{\int_0^{t_{cut}} FJE(\tau) d\tau}{L} \quad [46]$$

$$P_S = \frac{\int_0^{t_{cut}} FJE(\tau) d\tau}{L t_{cut}} \quad [47]$$

where t_{cut} is the time when the cutoff potential for the MH electrode is reached in a discharge. Note that both these quantities are defined with respect to the superficial volume, not the volume of the active material. In the latter case the factor $(1 - \epsilon)$ would be included.

Parameters

We simulate a MH electrode that corresponds to the ones produced by Finnish Oy Hydrocell, Ltd. These electrodes are characterized by their high capacity per cross-sectional area, 220 mAh/cm^2. With the void volume fraction of 0.3 and parameter values from Table I, this leads to the electrode thickness of about 1.5 mm.

The integral diffusion coefficient of KOH (in cm^2/s)

$$D^{free} = \exp(-10.467 - 8.1607c^{1/2} + 286.2c - 2539.8c^{3/2} + 7207.5c^2) \quad [48]$$

and the conductivity (in S/cm)

$$\sigma^{free} = c \exp(5.5657 - 6.1538c^{1/2} + 13.408c - 1075.8c^{3/2}) \quad [49]$$

where the concentration is in mol/cm^3, are from Ref. 3.

In the lack of reliable measurement data we choose the contact resistivity coefficient, ρ_c, in such a way that with Eq. 19 the conductivity of the solid phase is 150 S/m for particles having the radius of 10 μm, which leads to the value given in the table.

The reaction rates k_d and k_c correspond the initial equilibrium potential of −0.934 V [10] and exchange current density of 1.25×10^{-4} A/cm^2 Ref 1.

Table 1. General parameters.

Parameter	Value
c_{0_H}	6000 mol/m^3
D^H	5×10^{-15} m^2/s
h_0	77,400 mol/m^3
k_d	2.2118×10^{-6} m^4/mol s
k_c	4.2209×10^{-17} m/s
L	1.154812 mm
t_+	0.22
T	298 K
β	1.05
ϵ	0.3
ρ_c	8.47×10^{-8} Ω m^2
Φ_{Ni}	0.3 V vs. Hg/HgO

The electrode potential of the nickel electrode, Φ_{Ni}, is 0.3 V vs. Hg/HgO so that the open-circuit cell potential is 0.3 − (−0.934) = 1.234 V. In the same way, the cutoff potential of −0.6 V for the MH electrode corresponds the value of 0.9 V for the cell potential.

The diffusion coefficient of hydrogen is in good agreement with the values reported in Ref. 11 and the initial hydrogen concentration is about 1 wt %.

Simulations

Here the mathematical model is used to predict the discharge behavior of the cell under various conditions. The electrode is discharged with constant current until the cutoff cell potential of 0.9 V is reached.

Uniform particle size.—In this section we consider cases where the particle size is constant throughout the electrode. The effective conductivity of the solid phase depends on the particle radius according to Eq. 19.

We study electrodes having particle radii of 15, 10, 5, 2.5, 1, and 0.5 μm. In each case we apply three discharge current densities: 440 mA/cm^2 (2C rate), 220 mA/cm^2 (1C rate), and 100 mA/cm^2 (C/2.2 rate).

Cell potentials vs. state of discharge are shown in Fig. 2, 3, and 4. We can see that for all current densities it is advantageous to decrease the particles radius from 15 μm. This is a simple consequence of the fact that for the same porosity an electrode with smaller particles has more surface area and the relative speed of hydrogen diffusion is higher due to the shorter diffusion length. However, because the conductivity of the solid phase decreases with decreasing particle

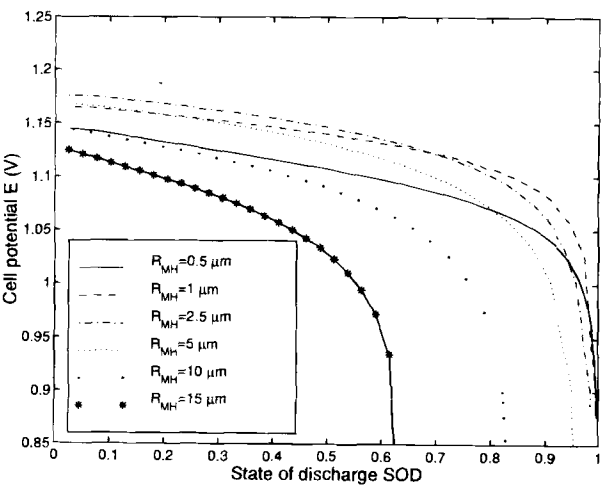

Fig. 2. Cell potential *E* for the C/2.2 rate (100 mA/cm^2). SOD is defined in Eq. 33.

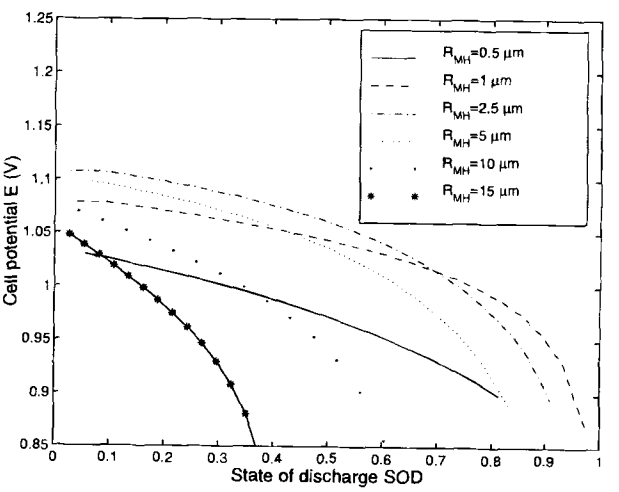

Fig. 3. Cell potential *E* for the 1C rate (220 mA/cm^2).

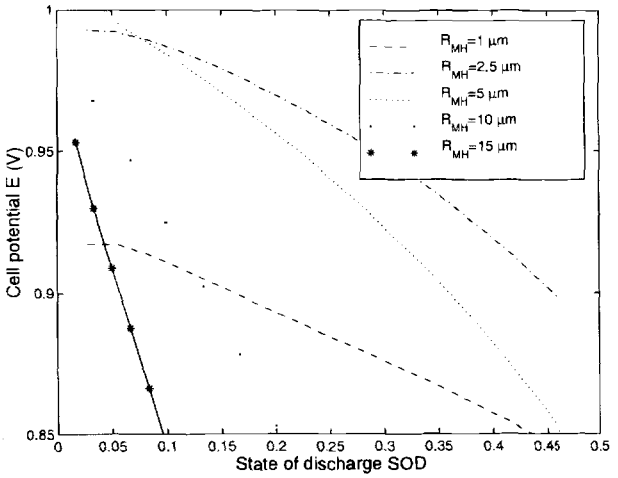

Fig. 4. Cell potential *E* for the 2C rate (440 mA/cm^2). The curve for 0.5 μm particles is not shown because the cutoff potential was reached almost immediately.

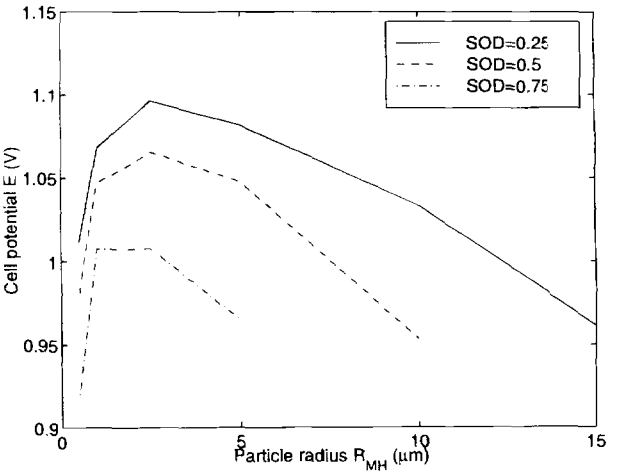

Fig. 6. Cell potential *E* vs. particle radius with the 1C rate for SOD values of 0.25, 0.5, and 0.75.

size, the smallest particles do not give the best electrode. As the discharge rate increases, this effect becomes more pronounced. Thus, for the C/2.2 rate (Fig. 2) the highest charge utilization is obtained for the electrodes with 1 and 0.5 μm particle radii, but the cell potential is lower for the latter. Initially, the 2.5 μm particle radius gives the highest cell potential. Then for the 1C rate (Fig. 3) both the utilization and the cell potential are considerably worse for 0.5 μm particles than for 1 μm particles, which give the best results. Again, for the values of state of discharge less than about 0.7, the highest cell potential is achieved with 2.5 μm particles. Finally, for the 2C rate (Fig. 4), the best electrode is the one with 2.5 μm particle radius. The curve for 0.5 μm particles is not plotted because the cutoff potential was reached almost immediately.

The same behavior is observed in the Ragone plot in Fig. 5. In general, for a given particle size as the discharge rate increases, the specific energy decreases and the average specific power increases. Moreover, the average specific power is practically independent of the particle size. For the rates of C/2.2 and 1C the electrode with 1 μm particle radius is the best, but for the 2C rate 2.5 μm particles give considerably higher specific energy. Also the effect of changing the particle size is greater when the discharge rate is higher.

More specifically, for C/2.2 and 1C rates the optimal particle radius (with respect to specific energy) is between 0.5 and 1 μm and for 2C rate the particle radius should be between 1 and 2.5 μm. Furthermore, for the 1C rate the optimum is closer to 1 μm than for the C/2.2 rate. That is, the optimal particle radius seems to increase with increasing discharge rate.

In Fig. 6 cell potential vs. particle radius is plotted for three values of state of discharge (SOD): 0.25, 0.5, and 0.75. The discharge rate is 1C. According to this diagram the cell potential is maximized when the particle radius is 2.5 μm.

To summarize we can say that with the parameter values and model for the solid phase conductivity used in the simulations, the best overall choice is the 2.5 μm particle radius. Note that we consider here a microencapsulated MH alloy, which is less susceptible to oxidiztion. Generally, as the particle size decreases there is increasing potential for the materials to get oxidized. With oxidization the results could change completely.

The particle size affects also the fundamental behavior of a MH electrode through its effect on the diffusion length of hydrogen.When the particles are big, the electrode is controlled by slow hydrogen diffusion, and it is ohmically controlled when the particles are small and hydrogen is readily available. This can be clearly seen in Fig. 7 and 8 where potential losses with 1C rate are plotted for 15 and 0.5 μm particles. With big particles the reaction overpotential and the polarization loss at the end of the discharge dominate, while the ohmic losses in the electrolyte and solid are more significant when the particles are small. Note that this change between the roles of ohmic and hydrogen-diffusion-related losses would remain even if

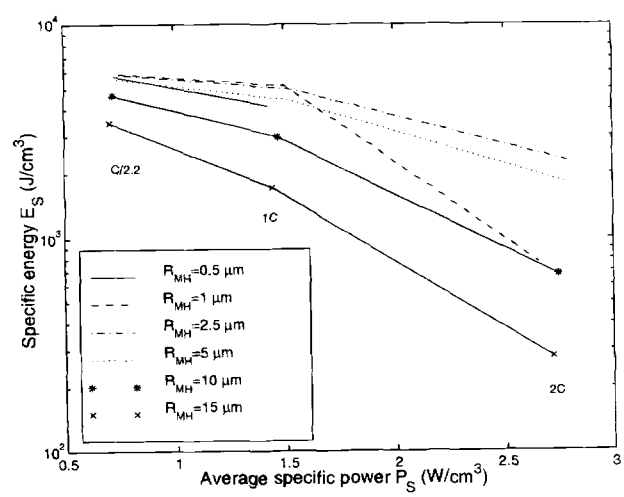

Fig. 5. Ragone plots (E_S vs. P_S) for various particle radii and discharge rates. Again, the case of 0.5 μm particles with the 2C rate is not plotted.

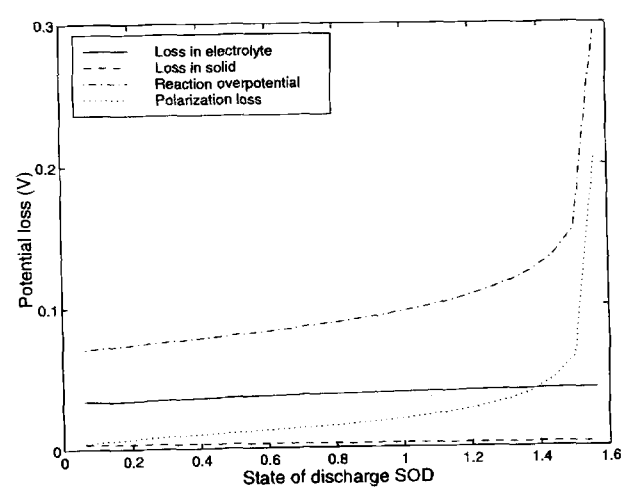

Fig. 7. Averaged potential losses $\bar{\eta}_l$, $\bar{\eta}_s$, $\bar{\eta}_r$, and $\bar{\eta}_p$ for the 1C rate and 15 μm particle radius.

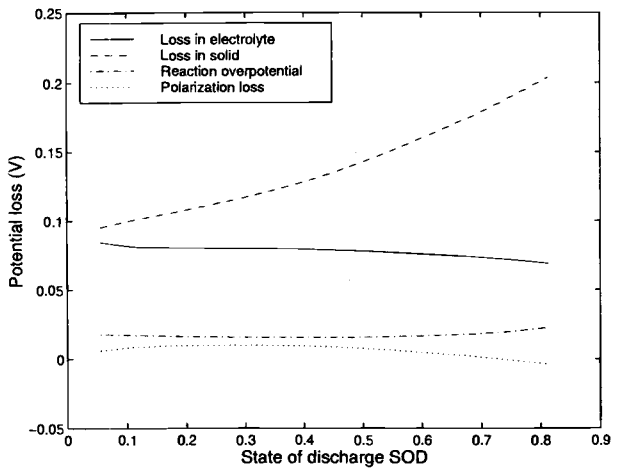

Fig. 8. Averaged potential losses $\bar{\eta}_l$, $\bar{\eta}_s$, $\bar{\eta}_r$, and $\bar{\eta}_p$ for the 1C rate and 0.5 μm particle radius.

the conductivity of the solid phase were independent of particle size. We exploit this fact in the next section.

Nonuniform particle size.—We now consider electrodes in which the particle size of the MH alloy varies from place to place. That is, the particle radius, R_{MH}, is a function of the longitudinal coordinate x.

In contrast with the preceding section, the conductivity of the solid phase is now taken independent of the particle size. In fact, we assume that the conductivity of the solid is very good. This is a reasonable assumption for a micro-encapsulated electrode.[1]

We keep the capacity and the total active surface area of the electrode fixed and find such a particle radius profile $R_{MH}(x)$ such that the electrode performance is improved.

The particle radius and active surface area density α are related by Eq. 1. We work with the surface area density and only in the end give the results in terms of the particle radius.

Let us first take a look at the three characteristic times of a MH electrode, as in Ref. 12. These are the maximal theoretical discharge time

$$t_{max} = \frac{(1 - \epsilon)Lh_0}{J} \qquad [50]$$

the characteristic time of hydrogen diffusion in the solid phase

$$t_s = \frac{R_{MH}^2}{D^H} \qquad [51]$$

and the characteristic time of the diffusion in the liquid phase

$$t_l = \frac{L^2}{\sqrt{\epsilon}D^{free}} \qquad [52]$$

As the thickness and the porosity of the MH electrode are kept constant, we have $t_l \approx 1250$ s. For discharge current densities between 440 mA/cm^2 (2C rate) and 100 mA/cm^2 (C/2.2 rate), 1800 s $\leq t_{max} \leq$ 7920 s. Finally, for $R_{MH} = 10$ μm $t_s = 20{,}000$ s, and for $R_{MH} = 0.5$ μm we have $t_s = 50$ s. Thus, depending on the discharge rate and on the particle size, the relative time scales of the processes in the electrode vary considerably.

If $t_s >> t_{max}$, the electrode is limited by the hydrogen diffusion. In this case the reaction is very evenly distributed throughout the electrode, especially in the middle stages of the discharge. This means, for example, that the potential loss in the electrolyte does not increase significantly with time and the reaction overpotential and the polarization loss dominate.

If, however, $t_s << t_{max}$, hydrogen is readily available and the potential loss in the electrolyte becomes important. The reaction proceeds as a relatively narrow zone and consequently, the potential loss in the electrolyte increases almost linearly with time.

In the latter case the electrode performance can be improved by suitably changing the surface area density within the electrode. Hence in this section we study an electrode in which the particle radius is 0.5 μm. The goal is to find such a surface area density profile that the reaction is as evenly distributed as possible. Spatially constant reaction rate density leads to constant potential loss in the electrolyte and in the solid. The more even consumption of hydrogen should also decrease the polarization loss.

Unfortunately, due to the nature of the problem, such a surface area density profile would not be independent of time. We can, however, use an approximative calculation to find a profile that still has beneficial effects to electrode performance.

Assume that the reaction rate density is constant, that is, for all x

$$\alpha(x)j(x) = \frac{J}{L} \qquad [53]$$

Then the flux density of hydroxyl ions is given by

$$J\left(1 - \frac{x}{L}\right) \qquad [54]$$

As t_{max} and t_l are of the same order of magnitude for the discharge rates we are interested in, it is reasonable to assume that the electrolyte concentration remains approximately at its initial value, c_0, and that the mass transport in the electrolyte is due to migration only. Thus the electrolyte potential satisfies

$$\frac{\sigma_-}{F}\frac{\partial}{\partial x}\phi = J\left(1 - \frac{x}{L}\right) \qquad [55]$$

which yields

$$\phi(t, x) - \phi(t, 0) = \frac{FJL}{\sigma_-}\left(\frac{x}{L} - \frac{1}{2}\left(\frac{x}{L}\right)^2\right) \qquad [56]$$

Note that in this calculation the conductivity, σ_-, is a constant because we assumed that the concentration is independent of x.

Next we assume that the surface concentration of hydrogen depends only on time. This is a valid assumption if the diffusion coefficient of hydrogen is infinite so that it is reasonably good because $t_s << t_{max}$. Moreover, we assume that the conductivity of the solid phase is infinite so that

$$\varphi(t, x) = 0 \qquad [57]$$

for all t and x. This assumption is not necessarily needed, but taking the effects of the positive conductivity and especially the particle size into account would make the calculations more complicated.

By discarding the charge part of the Butler–Volmer equation, Eq. 24, we can write

$$\frac{J}{L} = \alpha(x)k_d c_0 h_s(t)\exp\left(\frac{0.5F}{RT}V(t, x)\right) \qquad [58]$$

where

$$V(t, x) = -\phi(t, x) \qquad [59]$$

As the left side of Eq. 58 is independent of x, the same must hold for the right side as well. Consequently

$$\alpha(x)\exp\left(-\frac{0.5F}{RT}[\phi(t, x) - \phi(t, 0)]\right) = \alpha(0) \qquad [60]$$

or

$$\alpha(x) = \alpha(0)\exp\left(\frac{0.5F}{RT}[\phi(t, x) - \phi(t, 0)]\right) \qquad [61]$$

Substituting Eq. 56 into the previous equation, we obtain an expression for the surface area density as a function of x

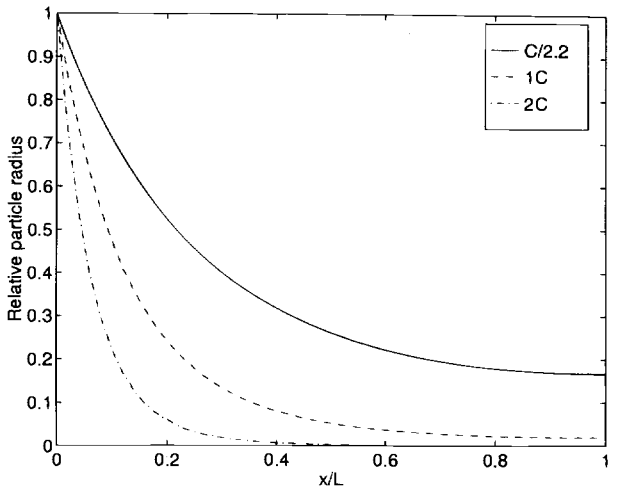

Fig. 9. Relative particle radius profiles $R_{MH}(0)/R_{MH}(x)$ for various discharge rates.

$$\alpha(x) = \alpha(0)\exp\left\{\frac{0.5F}{RT}\frac{FJL}{\sigma_-}\left(\frac{x}{L} - \frac{1}{2}\left(\frac{x}{L}\right)^2\right)\right\} \quad [62]$$

From Eq. 1 it then follows that

$$R_{MH}(x) = \frac{3(1-\epsilon)}{\alpha(x)} \quad [63]$$

The value of the surface area density at $x = 0$ is determined by requiring that that the total surface area be the same as with a constant 0.5 μm particle radius. In other words, we solve the equation

$$\frac{3(1-\epsilon)L}{0.5\,\mu m} = \alpha(0)\int_0^l \exp\left\{\frac{0.5F}{RT}\frac{FJL}{\sigma_-}\left[\frac{\xi}{L} - \frac{1}{2}\left(\frac{\xi}{L}\right)^2\right]\right\} d\xi \quad [64]$$

for $\alpha(0)$. The corresponding particle radii at $x = 0$ for C/2.2 and 1C rates are 1.87 and 11.46 μm, respectively.

Particle-size profiles for various discharge rates are shown in Fig. 9. According to the calculations, the particle size must decrease from the counter electrode if an evenly distributed reaction is wanted. This is easy to understand: if the reaction rate density is to be the same at both ends of the electrode, the larger electrolyte potential loss for the far end must be compensated by increasing the active surface area density there. This means decreasing the particle size. Furthermore, we see that the higher the current density the more the particle size must decrease. For C/2.2, the particle radius decreases from 1.87 to 0.31 μm and for the 1C rate, from 11.46 to 0.22 μm. For the 2C rate extreme reduction in particle size is required.

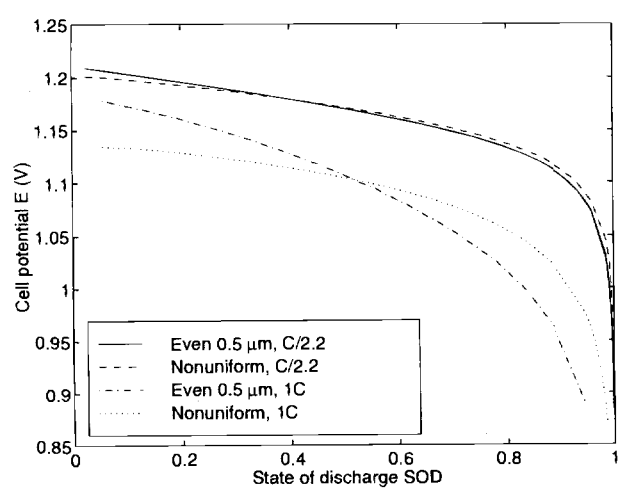

Fig. 10. Cell potential *E* for even 0.5 μm particle radius and a nonuniform particle size with C/2.2 and 1C rates.

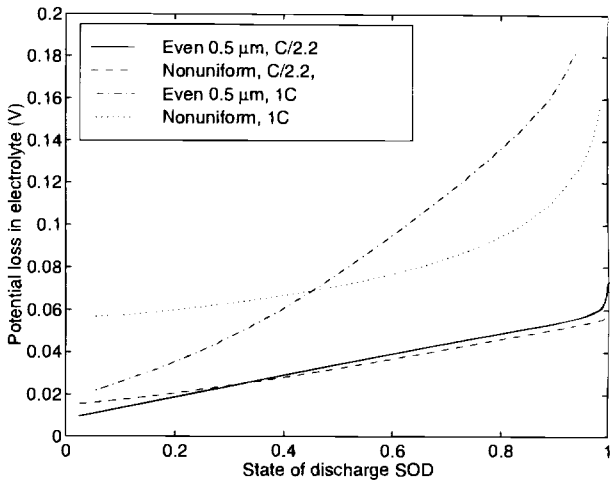

Fig. 11. Average potential losses in the electrolyte $\bar{\eta}_l$ for even 0.5 μm particle radius and a nonuniform particle size with C/2.2 and 1C rates.

In Fig. 10 an electrode with the above-derived nonuniform particle radius profile is compared with an electrode in which the particle size is constant. Both electrodes have the same capacity and total surface area. Two discharge rates, C/2.2 and 1C, are studied. For the lower discharge current density we see that the cell potentials are very close to each other. For the 1C rate, however, the utilization is about 5% higher for the nonuniform electrode. Another interesting phenomenon is that the nonuniform electrode gives a more stable cell potential, that is, the potential drops only about 55 mV during the first 70% of discharge when the corresponding drop for the uniform electrode is about 125 mV.

Figures 11 and 12, showing the average potential loss in the electrolyte and the uniformity of reaction, prove that we succeeded in making the reaction more even. The above-mentioned flatter electrode potential curve for the 1C rate is a consequence of the less rapidly increasing loss in the electrolyte.

The reaction overpotentials and the polarization losses are depicted in Fig. 13 and 14. We see that initially greater reaction overpotentials are needed for the nonuniform electrode. The increase, however, is compensated by decreases in other losses. As we suggested earlier, the polarization losses for the nonuniform electrode are most of the time lower due to the more even consumption of hydrogen. The

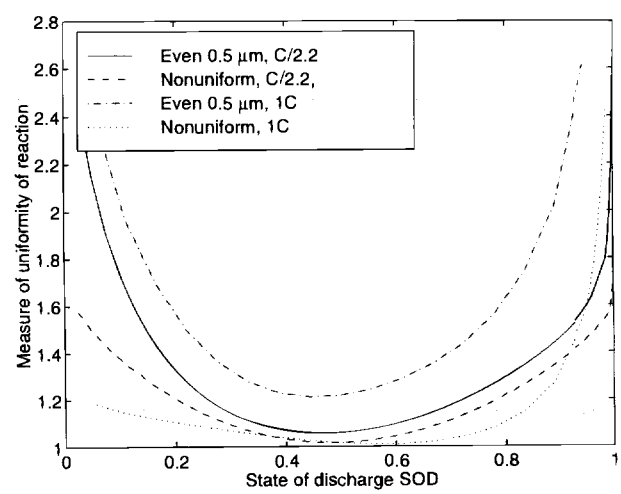

Fig. 12. Measure of uniformity of reaction M for even 0.5 μm particle radius and a nonuniform particle size with C/2.2 and 1C rates.

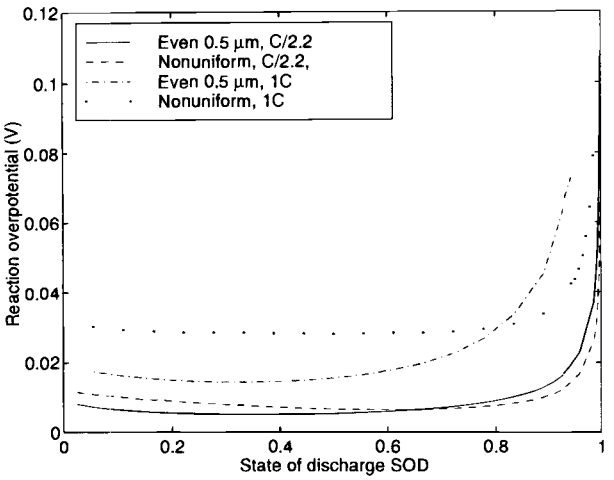

Fig. 13. Average reaction overpotentials $\bar{\eta}_r$ for even 0.5 μm particle radius and a nonuniform particle size with C/2.2 and 1C rates.

most important observation here is that the final steep increase in the reaction overpotential is delayed for the nonuniform electrode. This results in better utilization.

In general, we note that manipulating the particle size has greater influence on the electrode behavior when the current density is higher.

When trying to apply this to bigger particles, we failed, and it became clear that fast hydrogen diffusion is an essential prerequisite. Here it was obtained by decreasing the particle size, but for other kinds of electrodes larger diffusion coefficients in the solid phase may allow bigger particles. Values of the order of 10^{-13} m^2/s for the diffusion coefficient of hydrogen in MH alloys are reported in Ref. 13. As this value is about one hundred times larger than the one used in the simulations, the same relative speed of hydrogen diffusion would be achieved with a ten times larger particle radius, 5 μm.

Conclusions

From the simulation results it is clear that the particle size affects the electrode performance significantly. Moreover, the importance of the particle size increases with the discharge rate.

When the particle size is uniform and the conductance of the solid phase decreases as the particle size decreases, the optimal particle size increases with discharge rate.

Assuming that the conductance of the solid phase is very good and independent of the particle size, we showed that for a given total active surface area, better electrode performance can be achieved by distributing the surface area per unit volume nonuniformly. Especially for higher current densities it is advantageous to decrease the particle size away from the counter electrode, because this yields higher usage and more stable cell potential. It should be emphasized that this surface area distribution optimization works best for thick electrodes.

Note that it is difficult to manufacture an electrode with a specified nonuniform particle size. However, approximating a smooth profile with a layered structure should produce positive results as well.

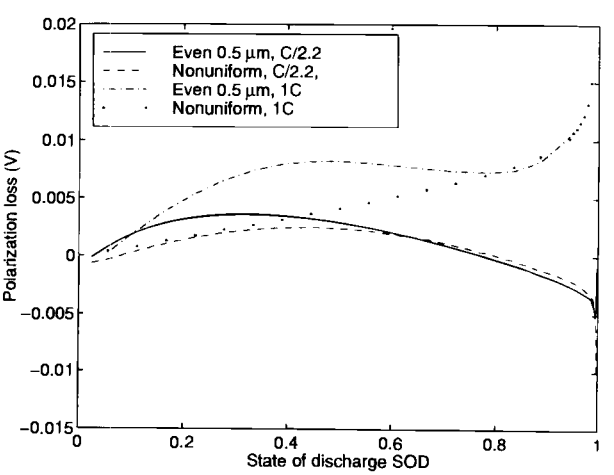

Fig. 14. Average polarization losses $\bar{\eta}_p$ for even 0.5 μm particle radius and a nonuniform particle size with C/2.2 and 1C rates.

Manuscript submitted September 23, 1997; revised manuscript received February 13, 1998.

The Helsinki University of Technology assisted in meeting the publication costs of this article.

LIST OF SYMBOLS

c	concentration of electrolyte, mol/m^3
c_0	initial concentration of electrolyte, mol/m^3
D	effective integral diffusion coefficient of KOH, m^2/s
D_H	diffusion coefficient of hydrogen in MH alloy, m^2/s
D^{free}	integral diffusion coefficient of KOH, m^2/s
D_+	effective diffusion coefficient of positive ions, m^2/s
D_-	effective diffusion coefficient of negative ions, m^2/s
D_+^{free}	diffusion coefficient of positive ions, m^2/s
D_-^{free}	diffusion coefficient of negative ions, m^2/s
E	cell potential, V
E_S	energy density, J/m^3
F	Faraday's constant, 96,500 C/mol
h	concentration of hydrogen in MH particles, mol/m^3
h_s	surface concentration of hydrogen on MH particles, mol/m^3
h_0	initial concentration of hydrogen in MH particles, mol/m^3
i_0	exchange current density in initial conditions, A/m^2
j	reaction rate density on MH particle surfaces, mol/m^{2}s
J	discharge current density, mol/m^2 s
k_c	charging reaction rate, m/s
k_d	discharging reaction rate, m^4/mol s
L	thickness of MH electrode, m
M	measure of uniformity of reaction
P_S	average power density, W/m^3
r	spatial coordinate in MH particles, m
R	universal gas constant, 8.3143 J/mol K
R_{MH}	radius of MH particles, m
SOD	state of discharge
t	time, s
t_{cut}	time when cutoff potential is reached, s
t_l	characteristic time of diffusion in electrolyte, s
t_{max}	maximal theoretical discharge time, s
t_s	characteristic time of diffusion in solid, s
t_+	transference number of positive ions
T	temperature, K
V	potential difference between solid and liquid phases vs. Hg/HgO, V
V_{loss}	total potential loss in MH electrode, V
V_0	equilibrium potential, V
x	spatial coordinate in MH electrode, m

Greek

α	surface area density of MH particles, 1/m
β	maximal relative charge level
ϵ	porosity of MH electrode
η_l	potential loss in electrolyte, V
η_p	polarization loss, V
η_r	reaction overpotential, V
η_s	potential loss in solid, V
$\bar{\eta}_l$	average potential loss in electrolyte, V
$\bar{\eta}_p$	averge polarization loss, V
$\bar{\eta}_r$	average reaction overpotential, V
$\bar{\eta}_s$	average potential loss in solid, V
κ	effective conductivity of solid, S/m
κ_0	conductivity of bulk MH alloy, S/m
ρ_c	contact resistivity coefficient of MH particles, Ω m^2
σ	effective conductivity of electrolyte, S/m
σ^{free}	conductivity of electrolyte, S/m
σ_+	effective ionic conductivity of positive ions, S/m
σ_-	effective ionic conductivity of negative ions, S/m
σ_+^{free}	ionic conductivity of positive ions, S/m
σ_-^{free}	ionic conductivity of negative ions, S/m
ϕ	electric potential in electrolyte, V

Φ_{MH} electrode potential of MH electrode, V
Φ_{Ni} electrode potential of nickel electrode, V
φ electric potential in solid, V
ξ integration variable corresponding to spatial coordinate x, m

REFERENCES

1. G. Zheng, B. N. Popov, and R. E. White, *J. Appl. Electrochem.*, To be published.
2. M. Viitanen, *J. Electrochem Soc.*, **140**, 936 (1993).
3. P. De Vidts, J. Delgado, and R. E. White, *J. Electrochem. Soc.*, **142**, 4006 (1995).
4. J. Heikonen, K. Vuorilehto, and T. Noponen, *J. Electrochem. Soc.*, **143**, 3972 (1996).
5. J. Newman and W. Tiedemann, *AIChE J.*, **21**, 25 (1975).
6. J. S. Newman, *Electrochemical Systems*, 2nd ed., Prentice Hall, Englewood Cliffs, NJ (1991).
7. G. Sewell, *Adv. Eng. Software*, **17**, 105 (1993).
8. J. Heikonen, Laboratory of Applied Thermodynamics Report No. 106, Helsinki University of Technology, Espoo, Finland (1997).
9. J. Heikonen, *J. Power Sources*, **66**, 61 (1997).
10. B. N. Popov, G. Zheng, and R. E. White, *J. Appl. Electrochem.*, **26**, 603 (1996).
11. G. Zheng, B. N. Popov, and R. E. White, *J. Electrochem. Soc.*, **142**, 2695 (1995).
12. T. F. Fuller, M. Doyle, and J. Newman, *J. Electrochem. Soc.*, **141**, 982 (1994).
13. T. Nishina, H. Ura, and I. Uchida, *J. Electrochem. Soc.*, **144**, 1273 (1997).

Thermocapillary Phenomena and Bubble Coalescence during Electrolytic Gas Evolution

Scott A. Guelcher, Yuri E. Solomentsev, Paul J. Sides,* and John L. Anderson

Department of Chemical Engineering, Carnegie Mellon University, Pittsburgh, Pennsylvania 15213, USA

ABSTRACT

Oxygen bubbles evolved in potassium hydroxide solution during electrolysis have been reported to be mutually attractive. A model based on thermocapillary flow and migration can explain the effect. A temperature gradient directed perpendicular to the electrode's surface into the liquid phase arises during electrolysis on a thin-layer electrode because of reaction overpotentials on the surface and ohmic losses within the electrode itself. This temperature gradient acts on a bubble at the electrode to produce a gradient of surface tension that drives flow of the adjacent liquid. Fluid next to the bubble flows away from the electrode, thus drawing liquid near the electrode laterally toward the bubble. A neighboring bubble is entrained in the thermocapillary flow and is convected toward the first bubble and vice versa. Furthermore, the presence of a bubble on a heated surface engenders a temperature gradient with a component parallel to the electrode's surface; neighboring bubbles undergo thermocapillary migration toward the bubble generating the gradient. Our theoretical model is compared with experimental data, and the agreement is good both qualitatively and quantitatively. The mutual approach of pairs of equal-size bubbles on the electrode can be modeled by considering only entrainment in each other's thermocapillary flow, because thermocapillary migration is unimportant; however, the motion of a smaller bubble toward a larger "collector" bubble can be described only when both entrainment and thermocapillary migration of the smaller bubble are included in the model.

Introduction

Bubble coalescence on an electrode surface during electrolytic gas evolution has long been identified as an important phenomenon.[1] Almost 20 years ago Sides and Tobias[2,3] studied the electrolytic evolution of oxygen bubbles from the back side of a vertically oriented transparent tin oxide electrode in alkaline electrolyte and discovered a characteristic behavior of bubbles they termed "specific radial coalescence." Large "collector" bubbles appeared to attract smaller "tracer" bubbles. A sequence of images from the film of Sides and Tobias demonstrating the effect appears in Fig. 1. The current density of oxygen evolution was 5 kA m^{-2}, and the electrolyte was 3% (mass) KOH. The frames were spaced in time by 0.4 ms, and the frame width was 200 μm. The bubbles appeared to be on the surface of the transparent antimony-tin oxide electrode and were growing away from the viewer. In the first frame, small tracer bubbles (1–6) surrounded a large collector bubble (lower left quadrant) in a nearly hexagonal arrangement. As time elapsed, each tracer bubble moved toward the collector bubble until it eventually coalesced with it. Other examples of specific radial coalescence appeared in the same frames. Two medium-size tracer bubbles (7 and 8) were attracted to another collector bubble and coalesced with it. In each case, the bubbles moved toward the collector bubble from all points around the large bubble; the effect therefore was independent of gravity, since gravity would have moved the bubbles uniformly in one direction. Furthermore, the effect was probably not due to natural convection because it was highly ordered; it occurred spontaneously on the electrode in many groups similar to the two groups in Fig. 1. This pattern of coalescence was an important chronologically intermediate step between single bubble growth and coalescence due to relative motion of very large bubbles driven by gravity. At about the same time and independently, Janssen and van Stralen[4] reported similar observations of lateral bubble motion on a transparent electrode during electrolytic gas evolution. This specific radial coalescence has never been explained satisfactorily.

We attribute specific radial coalescence to thermocapillary phenomena, that is, to the effects exhibited when temperature gradients engender gradients of interfacial tension. The primary temperature gradient in this case arises from conduction of excess heat away from the electrode into the liquid; the excess heat is produced by the reaction overpotentials at the surface and ohmic losses resulting from conduction within the thin-layer electrode. Thermocapillary migration and thermocapillary flow are two examples of thermocapillary phenomena. Thermocapillary migration, the motion of bubbles in a temperature gradient by virtue of a temperature-dependent surface tension, has been well documented.[5,6] We identify thermocapillary flow as the liquid motion that occurs when a bubble is held stationary (for example, by the electrode surface) in a temperature gradient; the gradient of surface tension of the stationary bubble forces motion of the liquid.

A schematic of thermocapillary flow appears in Fig. 2a. Two bubbles are on a wall that is hot relative to the bulk liquid. The gradient of surface tension of the liquid at the bubble surfaces, arising from the overall temperature gradient, drives flow of the liquid adjacent to each bubble;

* Electrochemical Society Active Member.